Data, exergy, and energy analyses of a vertical-bore, ground-source heat pump for domestic water heating under simulated occupancy conditions

Moonis R. Ally[1], Jeffrey D. Munk, Van D. Baxter, Anthony C. Gehl
Oak Ridge National Laboratory, Oak Ridge, Tennessee, USA[2]

Abstract

Evidence is provided to support the view that 68%-76% of the energy required to produce domestic hot water may be extracted from the ground which serves as a renewable energy resource. The case refers to a 345 m^2 research house located in Oak Ridge, Tennessee, 36.01° N 84.26°W in a mixed-humid climate with HDD of 2218°C-days (3993°F-days) and CDD of 723°C-days (1301°F-days). The house is operated under simulated occupancy conditions in which the hot water use protocol is based on the Building America Research Benchmark Definition which captures the water consumption lifestyles of the average family in the United States. The 5.3 kW (1.5-ton) water-to-water ground source heat pump (WW-GSHP) shared the same vertical bore with a separate 7.56 KW water-to-air ground source heat pump for space conditioning the same house. Energy and exergy analysis of data collected continuously over a twelve month period provide performance metrics and sources of inherent systemic inefficiencies. Data and

[1] Corresponding author: Tel.: 00+1+865-576-8003; fax: 00+1+865-574-8884
E-mail address: allymr@ornl.gov (M. R. Ally)

analyses are vital to better understand how WW-GSHPs may be further improved to enable the ground to be used as a practical renewable energy resource.

Key Words: Exergy, heat pump, thermodynamics, sustainability, ground-source

Nomenclature

Quantities

ACH	air changes per hour measured at differential pressure of 50 Pa
CDD	cooling degree days
C.V	Coefficient of Variance (dimensionless); a measure of dispersion
COP	coefficient of performance (dimensionless)
DOE	United States Department of Energy
DHW	domestic hot water
EWT	entering water temperature (K)
GL	Ground Loop
GSHP	ground source heat pump
GWP	global warming potential
HDD	heating degree days
HX	Heat Exchanger
g	gravitational acceleration ($m \cdot s^{-2}$)

h	enthalpy ($kJ \cdot kg^{-1}$)
$\dot{I}$	rate of thermodynamic irreversibility (W)
LWT	leaving water temperature (K)
$\dot{m}$	mass flow rate ($kg \cdot s^{-1}$)
Mtoe	million tons of oil equivalent
OEM	Original Equipment Manufacturer
P	pressure (kPa)
$\dot{Q}$	thermal energy flow (W)
QSSSF	Quasi-Steady-State-Steady Flow
R_{SI}	R-value, a measure of thermal resistance ($m^2 \cdot K \cdot W^{-1}$)
R_{US}	R-value, a measure of thermal resistance ($ft^2 \cdot {}^oF \cdot h \cdot Btu^{-1}$)
S.D	Standard Deviation, a statistical measure of dispersion
s	entropy ($kJ \cdot kg^{-1} \cdot K^{-1}$)
T	temperature (K)
U	internal energy in control volume (kJ)
V	velocity ($m \cdot s^{-1}$)
$\dot{W}$	rate of work (W)
WA-GSHP	water-to-air ground source heat pump
WW-GSHP	water-to-water ground source heat pump
$\%\Delta$	percent deviation
η	efficiency (dimensionless)
$\dot{\sigma}$	rate of entropy generation ($W \cdot K^{-1}$)

Subscripts

b	brine
Brine-HX	brine heat exchanger
comp.	pertaining to the compressor
comp. meas.	compressor quantity measured (actual)
CV	control volume
EWT	entering water temperature
i	inlet location
e	exit location or electrical energy
j	thermal reservoir other than the dead state or surroundings
o	dead state or surroundings
map	pertaining to the compressor map
Ref-Air HX	refrigerant-to-air heat exchanger

1. Introduction

A rigorous examination of using a vertical-bore ground source heat pump for domestic water heating is described in this paper. Although energy from the ground is freely available, its practical extraction from the ground for residential use is not yet widespread. The projected 2015 U.S. buildings sector energy end-use splits indicates that water heating alone would consume 7.47 x 10^{11} kWh of energy, accounting for 12.7% of total building energy consumption [1]. Carbon dioxide emission due to water heating in buildings is 2.041 x 10^{11} kg, of which 9.85 x 10^{10} kg is from electric water heating [2]. The total residential sector site energy consumption for water heating in 2015 is projected at 5.626 x 10^{11} kWh of which natural gas is the dominant fuel, accounting for 3.84 x 10^{11} kWh (68.2% of total) followed by electricity, 1.407 x 10^{11} kWh (25% of total), and the remainder being fuel oil, liquefied petroleum gas, and renewables. The 1.407 x 10^{11} kWh on site electricity consumption translates to 4.2 x 10^{11} kWh of source energy consumption. In terms of source energy consumption, water heating and space heating represent 13.7% and 27.9%, respectively of total residential energy use [3]. For the January-October 2014 period, residential gas storage water heater and residential electric storage water heater sales increased 3.6% and 5.7%, respectively, compared to shipments in the same period in the previous year reflecting a growing trend in recent years, following the 2009 recession.

The abundant energy available in the ground represents a potentially huge opportunity to satisfy present and future energy demands. Within Europe, 7100 TWh or 610 Mtoe annually is available from accessible depths of which 260 Mtoe per year lie under the surface of the EU27 [4]. In an effort to combat climate change, the EU Commissioners want a binding target to

reduce carbon dioxide emissions by 40% from 1990 levels by year 2030. To attain this target, approximately 27% of the EU's energy will need to come from renewable resources [5].

Similar emphasis is noted from other countries. Estimates of energy and CO_2 savings with ground source heat pumps (GSHPs) in 10 states in India are summarized by Sivasakthivel et al.[6]. Studies to investigate both space conditioning and water heating using ground source heat pumps with an emphasis on energy consumption in poorly and in well-insulated houses in the UK has been reported by Bagdanavicius and Jenkins[7]. An experimental study of GSHPs for space heating in a cold climate in Turkey by Ozyurt and Ekinci [8] yielded a COP between 2.43 to 3.55. A status review and comparison of GSHPs with other heating options is reported by Stuart et al.[9]. Performance of an experimental GSHP rig connected to a 120m deep, 150mm diameter vertical bore installed at Hebei University, China was investigated by Man et al. [10]. Energy and exergy analysis of combined GSHP whose evaporator component works as a photovoltaic-thermal collector has been investigated by Ozturk [11]. Hybridized variations of GSHPs for space conditioning and for water heating have been investigated by researchers in recent years with a focus on increasing the performance using solar energy in conjunction with the ground [12]-[15].

The use of various refrigerants such as a ternary mixture of R124/R142b/R600a (named HTR01), carbon dioxide, R410a, R134a and propane in water-to-water ground source heat pumps (WW-GSHPs) for domestic hot water production has been intensively investigated by several researchers [10], [16]-[20]. *Prima facie* it seems that greater emphasis is being placed on carbon

dioxide relative to the other refrigerants presumably because of its low global warming potential (GWP), low cost, ease of handling, and ability to produce domestic hot water (DHW) up to 80^{o}C, an indispensable level for certain commercial markets. The choice of refrigerants presents its own peculiar technical issues. For example, with carbon dioxide, water stratification in a tank is essential to attain high COP, and the overall COP is significantly higher for heating a tank full of cold water than it is for heating the same volume of warm water, a characteristic of refrigerants (like carbon dioxide) that must operate beyond their critical pressure.

A review of various models and systems of vertical bore GSHPs showing significant energy savings and applicability in cold and hot climates is discussed by Yang et al.[21]. Based on extensive experimental data as well as exergy and energy analyses of horizontal loop ground source heat pumps for space conditioning and for domestic water heating, Ally et al., [22]-[23] point out the hierarchy of systemic inefficiencies, performance metrics, and the opportunity for improvement. Between 68-76% of the total domestic water heating load can be harvested from the ground as shown by Ally et al. [22] . Clearly, there is a tangible environmental and societal opportunity in developing technologies that reduce electricity consumption and promote the use of renewable energy.

In this paper we present data and analysis of producing domestic hot water over a 12-month period from January through December 2012 at a 345 m^2 research house located in Oak Ridge, Tennessee, USA (36.01° N 84.26°W). The 5.3 kW WW-GSHP was charged with 1.597 kg (56.0 oz.

avoirdupois) R410A and shared the same 94.5 m vertical bore ground loop with a separate water-to-air ground source heat pump (WA-GSHP) used to deliver space conditioning loads. The WW-GSHP delivered approximately 227 L/day of hot water at 49°C under simulated conditions. The ground loop used a "brine" solution consisting of a mixture of propylene glycol and water in a 20% (v/v) mixture maintained at a pressure of approximately 275.8 kPa with a bladder-inflated pressure tank, a standard feature in all ground loop designs.

The data and analysis includes entering and leaving brine temperatures, energy extracted from the ground loop, delivered energy for domestic water heating, compressor electricity use, monthly aggregated run times, component-wise energy, exergy balances, and performance metrics. These extensive data may be used as an anchor for comparative studies conducted elsewhere.

2. Vertical-Bore Ground Loop and Heat Pump

The shared vertical-bore is made of high density polyethylene (HDPE) tube, 0.019 m internal diameter inserted vertically into the ground to a depth of 94.5 m returning to the surface in a U-tube with total length of 189 m and a total surface area of 11.3 m^2. The arrangement of the vertical-bore and the WW-GSHP components are shown in Figure 1. The 5.3 kW WW-GSHP is rated at a COP of 3.1 based on a source entering water temperature (EWT) 0^oC and load EWT of 37.8^oC. The WW-GSHP was connected to a 303 L seamless, blow-molded, polybutylene hot water tank, impervious to rust and corrosion, equipped with 4.5 kW upper and lower heating elements for backup energy needed in case the WW-GSHP was inoperable due to an equipment

fault. The tank's rated energy factor (EF) for conventional electric resistance operation was 0.92.

The hot water use pattern is based on the research of Hendron and Engebrecht [24] segmented by use in showers, laundry, and dishwashing as shown in Table **1**. Running four cycles per week, the dishwasher's average hot water consumption was 15.3 L per wash. The clothes washer averaged 13.9 L of hot water per cycle and operated six cycles per week.

3. Equipment, Sensors and transducers

A schematic of the WW-GSHP components and its connection to the vertical-bore ground source loop and the hot water tank are shown in Figure 1. Numbered items in the refrigerant loop within the control volume (CV) refer to locations where measurements were made. With reference to Figure 1, the compressor suction (1) and discharge (2) pressures were measured with pressure transducers with an accuracy of ±0.25% of full scale (FS) mounted on Schrader ports. Leaving and entering water temperatures at locations (7) and (8), respectively, in the vertical-bore ground loop were measured with thermistors placed in wells. Temperatures at all other locations were measured with surface mounted thermistors that were first coated with conductive paste then attached to their respective locations with electrical tape, insulated with cork, and taped once again for good adherence. The thermistors had a time constant of 15s, and an accuracy of ± 0.2°C. A turbine meter with accuracy of ±2% over the calibrated flow range measured the brine flow rate. Domestic hot water flow rate was measured with a differential pressure transducer with ± 0.25% FS accuracy. Electrical power to the compressor, brine, and

DHW pumps were measured with instrumentation-grade transducers with split-core current transformers having a minimum accuracy of ± 0.45% of reading plus 0.05% of FS. Pressure drops in the connecting refrigerant lines were accepted as 1-1.5% of upstream pressure, as provided to us by the original equipment manufacturer (OEM).

4. Data Collection and Analysis

A data logger was programmed to collect data every 30 seconds, then average and store the collected data in 15 minute intervals before exporting it to a spreadsheet for post-processing and analysis. The thermistor dissipation factor (the quantity of energy required to raise its temperature by 1°C) and thermal time constant are 2 $mW \cdot C^{-1}$ and 15 s, respectively. With a sampling rate of 30 seconds, the temperature readings are deemed to be quasi-steady-state, steady-flow (QSSSF), justified on the basis that the state points were observed to reach constant values typically within 3-5 minutes of compressor run times. In the domestic hot water heat exchanger, the hot water temperatures at locations 9 and 10 reached steady state values between 1-4 minutes, depending on the temperature of the water in the tank at the start of the water flow to the DHW heat exchanger. Since compressor run times are much longer than 1-4 minutes, the assumption of QSSF is deemed valid in our analysis. Thermodynamic state points were evaluated using the National Institute of Standards and Technology (NIST) Reference Fluid Thermodynamic and Transport Properties Database (REFPROP) Version 8.0 [25]. Uncertainty in the calculated COPs is estimated to be ± 0.254. The monthly COPs are weighted average values based on compressor run times for the particular month.

5. Mass and energy balances

Under QSSSF conditions, the general mass balance equation is given by:

$$\frac{d\dot{m}}{dt} = \sum_e \dot{m} - \sum_i \dot{m} \cong 0 \qquad (1)$$

Applying Eqn. (1) to the brine solution in the vertical-bore ground loop between state points 7 and 8 under QSSSF conditions yields the brine mass flow rate $(\dot{m}_b)_e = (\dot{m}_b)_i = \dot{m}_b$. Similarly, application of Eqn. (1) between any two state points on the refrigerant loop, under the same QSSSF assumption gives the refrigerant mass flow rate in the refrigerant loop (points 1,2,…..6,1). In the absence of any direct measurement of the refrigerant mass flow rate in the system, it was calculated in three discreet ways: (1) through mass and energy balances around the ground loop (GL) heat exchanger (HX); (2) mass and energy balances around the DHW heat exchanger; and (3) using compressor maps supplied by the OEM.

The general energy balance equation [26], applied to arbitrarily chosen state points is given by:

$$\dot{Q}_o + \sum_j \dot{Q}_j + \dot{W} + \sum_{in} (h + \frac{V^2}{2} + gz)\dot{m} - \sum_{out} (h + \frac{V^2}{2} + gz)\dot{m} = \frac{dE_{CV}}{dt} \qquad (2)$$

where $\dot{Q}_o$ is the thermal energy exchanged with the surroundings at T_o. The thermal energies represented by $\dot{Q}_j$ are energy exchanges with any additional reservoir(s) at temperatures $T_1, T_2, T_3 \ldots T_j$, respectively; $\dot{W}$ is the rate of work (mechanical and/or electrical) input; h,V^2/g, gz represent enthalpy, kinetic, and potential energy terms, respectively; and $\dot{m}$ is the mass flow rate of refrigerant or of brine, as the case may be. The term, dE_{CV}/dt represents the rate of energy accumulation within the control volume of interest and is set to zero under the assumption of QSSSF invoked in the analysis; $E_{CV} = U + (1/2)V^2 + gz$ where U is the internal

energy of the mass within the control volume. Both, work ($\dot{W}$) and heat ($\dot{Q}_o, \dot{Q}_j$) terms are defined as positive in Eqn.(2) [26][27]for energy transfer *into* the CV.

Mass and energy balances around GL HX and DHW HX

Applying Eqns. (1) and (2) to the refrigerant side in the GL HX between state points 5 and 6 and then again to the brine side between points 7 and 8 yields the refrigerant mass flow rate estimate, $\dot{m}_{r,b}$ based on mass and energy balances around this heat exchanger yielding,

$$\dot{m}_{r,b} = \frac{\dot{m}_b (h_7 - h_8)}{(h_6 - h_5)} \tag{3}$$

Similarly, applying Eqns. (1) and (2) to the refrigerant side between state points 3 and 4 on the refrigerant loop, and once again between points 9 and 10 on the DHW side yields the refrigerant mass flow rate estimate, $\dot{m}_{r,DHW}$ based on the mass and energy balances around the domestic hot water heat exchanger yielding,

$$\dot{m}_{r,DHW} = \frac{\dot{m}_{DHW} (h_{10} - h_9)}{(h_3 - h_4)} \tag{4}$$

The refrigerant mass flow rates from Eqns.(3) and (4) as well as that obtained from the compressor map, $\dot{m}_{map}$ (provided by the manufacturer) are found to be in reasonable agreement, as shown in the respective columns in Table **2**. The percentage error between $\dot{m}_{map}$ and $\dot{m}_{r,DHW}$ ($\%\Delta_1 = (\dot{m}_{r,DHW} - \dot{m}_{map}) * 100 / \dot{m}_{map}$) is less than the percentage error between $\dot{m}_{map}$ and $\dot{m}_{r,b}$ ($\%\Delta_2 = (\dot{m}_{r,b} - \dot{m}_{map}) * 100 / \dot{m}_{map}$) because the relative errors in temperature

measurement are larger on the brine side where the temperature differences between LWT and EWT are less than they are for the DHW side where the temperature differences in both the refrigerant and water streams are larger. Since differences between LWT and EWT are typically 3-5°C and the accuracy of the temperature measurement is no greater than ±0.2°C, the brine side discrepancy $\%\Delta_2$, is greater than $\%\Delta_1$. All our analyses are based on refrigerant mass flow rates obtained from the compressor map, as supplied by the OEM.

Energy Analysis and COP

Under our QSSSF assumption, the mass balances become trivial with mass inflows equal to mass outflows. The monthly averaged energy balances for the WW-GSHP are presented in Table **3**. The total energy input terms are given by:

$$E_{in} = W_{e,Brine\,Pump} + W_{e,Comp.} + W_{e,DHW\,Pump} + W_{e,Aux.} + W_{e,Controls} + Q_{0,ground} \quad (5)$$

The total energy output terms are given by:

$$E_{out} = Q_{DHW} + Q_{0,Comp.} + losses \quad (6)$$

Referring to Table **3**, the percent difference between energy input and output, ($\%\Delta = (E_{in} - |E_{out}|)100/E_{in}$) is less than 6%, demonstrating reasonable goodness of data. Also note that the energy input (E_{in}) is greater than the absolute value of the energy output ($|E_{out}|$), with the difference attributed to energy losses.

The compressor energy consumption is highest in the winter (121.5 kWh in January) and lowest during the summer (66.1 kWh in July). More heat is extracted from the ground during winter (298.8 kWh in January) than during summer (232.6 kWh in July), for water heating. The energy needed for water heating is also highest in the winter (376 kWh in January) and lowest during

the summer (268 kWh in July). Referring to Table **4**, the water heating COP shows gradual improvement from winter to summer as EWTs increase gradually. Virtually no supplemental resistance heating was needed for water heating. The tank resistance heaters are turned on only during a "lockout" fault at the WW-GSHP, otherwise all the necessary heat is supplied by the WW-GSHP to produce hot water.

The water heating COPs in Table **4** take into account electrical energy consumed by the compressor, brine, and the DHW pumps as defined by,

$$COP = \frac{Q_{DHW}}{(W_{e,Brine\ Pump} + W_{e,DHW\ Pump} + W_{e,Compressor})} \quad (7)$$

Implicit in Eqn. (7) is the dependence of COP on EWT and LWT, both determinants in the amount of thermal energy extracted from the ground to make hot water. The monthly averaged EWT and LWT given in Table **4** support the fact that COP rises with increasing EWT. The brine and DHW pumps combined used a maximum of 11% of the total monthly electrical energy input (in January). Although the brine and DHW pumps did not operate near their optimum efficiency, these data suggest that pump efficiency is unlikely to be a dominant factor in improving GSHP performance, at least for the size range, climate, and use patterns prevalent in this study.

Of quintessential significance is the last column in Table **4** showing that 79% to 87% of the water heating energy comes from the ground, making GSHP technology a viable option for efficient utilization of the ground as a renewable energy resource. Further investigation of the sources of *systemic inefficiencies* is identified through Exergy analysis.

6. Exergy analysis

The general entropy balance equation [26] applied between various state points in Figure 1 is:

$$\dot{\sigma}_{total} = \sum_{out} \dot{m}s - \sum_{in} \dot{m}s - \frac{\dot{Q}_o}{T_o} = \sum_{j} \frac{\dot{Q}_j}{T_j} \geq 0 \tag{8}$$

where $\dot{\sigma}_{total}$ is the sum of the entropy generation rates due to internal irreversibilities and those due to irreversible heat transfer between the particular control volume encompassing the state points, and the surroundings.

The irreversibility (or equivalently, the availability) is a thermodynamic measure of the lost opportunity of doing useful work. Thermodynamic irreversibility, is given by:

$$\dot{I} = T_o \dot{\sigma} \quad or, \quad \dot{I} = T_j \dot{\sigma} \tag{9}$$

with T_o (or T_j) being the temperature of the surroundings of the particular control volume under consideration. Eqns. (1), (2), (8) and (9), when applied to the control volumes encompassing the particular initial and final states, yield the necessary mass, energy, and entropy balances to quantify the extent of irreversibility, or availability destruction. The sum of all the availability destructions around the closed refrigerant cycle constitutes its systemic inefficiency.

Compressor

Extending the control volume of the compressor to the surroundings and noting that no heat reservoirs other than the surrounding atmosphere are in contact with this control volume essentially implies that ($\dot{Q}_j$=0 but $\dot{Q}_o \neq 0$). This control volume includes the initial and final

state points 1 and 2, respectively. Applying Eqns. (1), (2), (8) and (9) to the control volume encompassing these two state points gives:

$$\dot{Q}_o = \dot{m}_{map}(h_2 - h_1) - \dot{W}_e \tag{10}$$

$$\dot{\sigma} = \dot{m}_{map}(s_2 - s_1) - \frac{\dot{Q}_o}{T_0} \tag{11}$$

$$\dot{I} = \dot{\sigma} T_o \tag{12}$$

The compressor energy transfer and irreversibility rates between the discharge (final state 2) and suction (initial state 1) ports, and the compressor run times are shown in Table **2**. The compressor irreversibility remains fairly constant throughout the months, but the compressor heat rejection rates to the surroundings varies from a minimum of 352.4 W in February to a maximum of 546.5 W in July. Compressor heat rejection to the conditioned space is a benefit during the heating season, but a disadvantage during the cooling season. The ratio, $\dot{I} / \dot{W}_e$ depicting irreversibility per unit electrical input to the compressor, remains fairly even, between 0.348 and 0.380 throughout the year, whereas the ratio $\dot{Q}_o / \dot{W}_e$ was low during the winter (February) and peaked in July as shown in **Figure 2**. These ratios respectively, are a measure of Lost Work and heat dissipated to the surroundings for every unit of electricity consumed by the compressor. Both ratios should be small if electricity is used efficiently. The

normalized ratio, EWT/EWT_{max}, is 1.0 in July, tapering off slightly on either side like a "bell curve" with a C.V. of 2.55%

Compressor discharge line to DHW Heat Exchanger

The control volume for the compressor discharge line (insulated) to the DHW HX encompasses state points 2 and 3 in **Figure 1**. The general mass, energy, and exergy balance Eqns. (1), (2), (8) and (9) applied to this segment reduce to:

$$\dot{Q}_o + \dot{m}_{map}(h_2 - h_3) = 0 \tag{13}$$

$$\dot{\sigma} = \dot{m}_{map}(s_3 - s_2) - \frac{\dot{Q}_o}{T_o} \tag{14}$$

$$\dot{I} = \dot{\sigma} T_o \tag{15}$$

With less than perfect insulation, some heat loss to the surroundings is expected, yielding $\dot{Q}_o$ slightly negative (-22.2W) and $h_2 \approx h_3$ with h_2 slightly greater than h_3. Since the connecting line is short, and the magnitude of the energy transfers and entropy production rates, $\dot{\sigma}$ are small compared to the entire cycle, they do not materially impact the overall analysis or conclusions.

Refrigerant-DHW Heat Exchanger

The control volume of the refrigerant line in the DHW HX encompasses the segment between initial and final state points 3 and 4, respectively. Applying the general mass, energy and entropy balances, Eqns. (1), (2), (8) and (9) gives for this segment:

$$\dot{Q}_o + \dot{m}_{map}(h_3 - h_4) = 0 \tag{16}$$

$$\dot{\sigma} = \dot{m}_{map}(s_4 - s_3) - \frac{\dot{Q}_o}{\frac{1}{2}(T_9 + T_{10})} \tag{17}$$

$$\dot{I} = \dot{\sigma} T_o; \quad T_o = \tfrac{1}{2}(T_9 + T_{10}) \tag{18}$$

where $\dot{Q}_o$ is <0 because heat is transferred from the refrigerant to the DHW tank. The entropy generation, irreversibility, and heat transferred to make hot water are tabulated in Table **2**. The values for T_9 and T_{10} are given in Table **5**.

Expansion valves and connecting lines

The control volume for the expansion valve and connecting lines encompass state points 4 and 5. The expansion valve is assumed to be adiabatic. The general mass, energy, and entropy balance equations applied to this segment yields:

$$\dot{Q}_o = \dot{m}_{map}(h_5 - h_4); \quad \dot{Q}_o = 0 \ (adiabatic) \tag{19}$$

$$\dot{\sigma} = \dot{m}_{map}(s_5 - s_4) \tag{20}$$

$$\dot{I} = \dot{\sigma} T_o \tag{21}$$

As shown in Table **2**, valve irreversibility is high (because the refrigerant pressure drop across the valve produces no useful work), but it is not as high as compressor irreversibility.

Refrigerant-GL HX

The control volume of the refrigerant to ground loop heat exchanger (GL HX) is on the refrigerant line encompassing initial and final state points 5 and 6, respectively. The general mass, energy and entropy balance equations applied to this control volume yields:

$$\dot{Q}_o = \dot{m}_{map}(h_6 - h_5) \tag{22}$$

$$\dot{\sigma} = \dot{m}_{map}(s_6 - s_5) - \frac{\dot{Q}_o}{\frac{1}{2}(T_{EWT} + T_{LWT})} \tag{23}$$

$$\dot{I} = \dot{\sigma} T_o;\ T_o = \tfrac{1}{2}(T_{EWT} + T_{LWT}) \tag{24}$$

where $\dot{Q}_o$ >0 because heat is transferred from the ground to the refrigerant. The rates of entropy generation, irreversibility, and heat transfer are tabulated in Table **2**. T_o is the average

of the EWT and LWT where, EWT= T_7 and LWT = T_8. The values for EWT and for LWT are shown in Table **5**. The highest and lowest rates of energy transfers with the ground occurred in July (5.016 kW) and in January (3.312 kW), respectively. The irreversibility rate $\dot{I}$, was high during June-August (cooling season) and lower during December-February (heating season), with cooling season irreversibility about two times greater than during the heating season. With highest heat uptake from the ground during the cooling season and high irreversibility, there appears to be an opportunity to improve the heat exchanger design.

Refrigerant line from GL HX to compressor

The control volume for the refrigerant line from the GL HX to the compressor suction line (insulated) encompasses initial and final state points 6 and 1, respectively, in **Figure 1**. The general mass, energy, and exergy balance equations for this line reduce to:

$$\dot{Q}_o = \dot{m}_{map}(h_1 - h_6) \tag{25}$$

$$\dot{\sigma} = \dot{m}_{map}(s_1 - s_6) - \frac{\dot{Q}_o}{T_o} \tag{26}$$

$$\dot{I} = \dot{\sigma} T_o \tag{27}$$

For this segment, the thermal exchange with the surroundings, $\dot{Q}_o$ is small, of the order of 30-40 W per month on average and the rate of entropy generation, $\dot{\sigma}$ is also small, of the order of 4x

10^{-3}W·K^{-1} on average resulting in a total monthly irreversibility rate of the order of 1 to 2 W. The refrigerant line from the compressor discharge to the DHW heat exchanger discussed above has comparable values of $\dot{Q}_o$, $\dot{\sigma}$ and $\dot{I}$.

7. Entropy production and irreversibility analysis

The sources of inefficiencies as measured by entropy generation and irreversibility in the refrigeration loop (1-2,…,6-1) in **Figure 1** are quantified and summarized in Table **6**. For any given month, the main source of systemic inefficiency is the compressor. In eight of the twelve months the expansion valve irreversibility exceed that of the GL HX and was slightly less in the remaining four months (June-Sept) of the year. The magnitudes of entropy and irreversibility rates of the connecting lines are negligible (less than 1%). The total irreversibility representing the actual amount of lost work is the product of the irreversibility rate and the compressor run time, tabulated in Table **7**. Although irreversibility rates $\dot{I}$, are lower during winter than in summer, the total lost work ($\dot{I} \times t_{Comp.}$) is highest during the winter months and lowest during the summer months because of higher compressor run times in winter than in summer (Table **7**).

Longer compressor run times in winter as compared to summer is understandable because both the supply water temperatures as well as the EWT are lower in winter than during the summer causing the compressor to run longer in the former season than in the latter to provide the necessary hot water at 49^{o}C. However, higher irreversibility rates , $\dot{I}$, in summer shown in

Table **7** appears *prima facie*, counterintuitive because higher summer EWTs result in higher COPs as distinctly shown in Table **4**. The question of why irreversibility is higher in summer when the COP is also high begs an explanation. The clue to resolving this apparent contradiction lies in the values of the Carnot efficiency (Table **4**) which is highest in summer and lowest in winter as should be expected because the difference between summertime EWTs and the hot water set point temperature are smaller in summer than they are in winter. Although the COPs in summer are higher than in winter, the COP relative to an ideal Carnot machine is the poorest in summer than in winter as depicted by the parameter, η (Table **8**). This relative poorer performance of the WW-GSHP reflected in the irreversibility rates displayed in Table **7** explains the apparent contradiction, raised above.

The sum of the rate of work input of an ideal compressor, $\dot{W}_{Carnot}$(Carnot engine power consumption) plus the rate of lost work, $\dot{I}_{Total}$ due to irreversibility within the control volume of the compressor must equal the rate of electrical work consumed by the actual compressor, $\dot{W}_{Compressor}$. The Carnot engine power is calculated on the basis of a two temperature (2-T) Carnot engine operating between the brine to refrigerant heat exchanger (GL HX) and the refrigerant to DHW HX. Since a 2-T Carnot engine is being considered and the temperatures in both DHW HX and GL HX vary, the average of the EWT and LWT is taken as the temperature at which heat is extracted from the ground, and the average of temperatures T_9 and T_{10} to which heat is rejected in DHW HX to generate hot water. If irreversibility is calculated correctly, then Eq. (28) must be satisfied within reasonable experimental error:

$$\dot{W}_{Comp..} = \dot{W}_{Carnot} + \dot{\sigma}_{Total} T_o = \dot{W}_{Carnot} + \dot{I}_{Total} \tag{28}$$

where $\dot{W}_{Carnot}$ is calculated as follows:

$$\dot{W}_{Carnot} = \frac{\dot{Q}_{Brine\ GL\ HX}}{COP_{Carnot}} \tag{29}$$

The Carnot COP is calculated in the usual manner:

$$COP_{Carnot} = \frac{(T_9 + T_{10})/2}{\left[\frac{(T_9 + T_{10})}{2} - \frac{(LWT + EWT)}{2}\right]} \tag{30}$$

If the irreversibility calculations are valid, then there should be good agreement, within experimental error, between the actual (measured) compressor power consumption, $\dot{W}_{Comp.meas.}$ and that calculated using Eq.(29). The goodness in agreement is given by the relative percent difference $\%\Delta = \left[(\dot{W}_{Comp.} - \dot{W}_{Comp.meas.})/\dot{W}_{Comp.}\right] \times 100$ (Table **8**). The Carnot work, $\dot{W}_{Carnot}$ is the minimum work required by the compressor whereas, $\dot{W}_{Comp.meas.}$ is the actual work consumed by the compressor. The measured compressor work relative to the Carnot work is defined as $\eta = [\dot{W}_{Carnot}/\dot{W}_{Comp.meas.}]$.

Monthly data in Table **8** tabulates the agreement between measured compressor power, $\dot{W}_{Comp.meas.}$ and that computed from Eq.(28), validating the irreversibility calculations within

acceptable experimental errors. The averaged compressor efficiency is 29% (±2.14%) of an ideal Carnot engine operating between the same temperatures, and remains rather consistent over the 12-month period. These performance metrics for domestic water heating agree very closely with a complementary field study by Ally et al. [22] using a horizontal ground loop in the same geographical area.

8. Discussion

The entire hot water demand specified by the Building America Benchmark Definition [24] which attempts to capture the living habits of the average household in the U.S and how they impact energy consumption was met with a 5.3 kW WW-GSHP connected to a 90.5 m vertical bore ground loop that also serviced space conditioning needs via a separate heat pump. The house is situated in U.S. Department of Energy (DOE) climate region 4 (mixed-humid) with coordinates, 36.01°N 84.26°W. The daily hot water needs are approximately 227 L/day at a temperature of 49^{o}C. The WW-GSHP serviced a 303 L capacity hot water tank with two 4.5 kW heating elements for backup, if necessary.

The highest averaged monthly COP achieved was 3.57 in July with an EWT of 28.0^{o}C. The lowest COP of 2.69 was in January with an EWT of 7.43^{o}C. The COPs are calculated on the basis of total energy input because that is what the consumer ultimately pays for in utility bills. Although the *rate* of energy extracted from the ground, $\dot{Q}_0$ is higher in the summer than in the winter (Table **2**: Refrigerant-Brine GL HX), the least amount of energy (233 kWh) was extracted from the ground in July (Table **3**: $\dot{Q}_{0,ground}$) and the most energy (299 kWh) extracted in

January to make hot water because of three reasons: (a) the incoming city supply water temperature is higher during the summer and therefore requires less energy to heat up to 49^{o}C than in the winter, (b) the compressor run times are less in summer than in the winter and (c) since the ground loop is shared for space conditioning as well, it had to service both needs when both were used simultaneously.

The energy balance equation was verified within 5.08% (S.D = ±0.43%) on average. Generally, the energy balances showed higher discrepancies (Table **3**: $\%\Delta$) during winter months due to the larger measurement errors in the smaller temperature differences between the EWT and the LWT.

The ground is unequivocally a useful source of renewable energy for water heating – providing abundant water heating energy year round (Table **3**: $\%Q_{GLHX}/|Q_{DHW}|$).

The monthly compressor heat rejection was found to be between 24 kWh-39 kWh (Table **3**) with negligible net benefit (in winter) or penalty (in summer) to conditioned space.

Although 86-88% of the total *electrical* energy input is consumed by the compressor (Table **3**), it represents only about 21-27% of the total *energy* input of the WW-GHSP for water heating (Table **3**) - the balance is extracted from the ground. A strong argument may be made for using the ground as a renewable energy source for domestic water heating.

The WW-GSHP operates at approximately 0.25-0.31 of the efficiency of a 2-T Carnot heat pump (Table **8**). This level of comparative efficiency remained fairly consistent throughout the 12-month field study. The greatest source of systemic inefficiency from the standpoint of the Second Law is the compressor. Although the rate of heat transfer from the ground to the brine

is lower in winter than in the summer (Table **8**), more heat (299 kWh) is extracted from the ground during winter than in summer (233 kWh) (see Table **3**) because of the lower city water supply temperature. Compressor energy consumption was highest in January (121.5 kWh) and lowest in July (66.1 kWh) primarily because of lower supply and EWT in winter than in summer. Since total lost work, $\dot{I}\ x\ t_{Comp.}$ is higher in winter (77.5 kWh) than in summer (47.6 kWh), the consumer pays more for *systemic* inefficiency during winter than in summer. These data for the vertical bore GSHP are supportive of, and are in excellent agreement, with a complementary field study on a horizontal bore GSHP [22],[23],[28] system as part of a comprehensive field work undertaken under the sponsorship of the U.S. Department of Energy.

9. Conclusions

The comprehensive 12-month field study demonstrated that a 5.3 kW WW-GSHP can service up to 227 L/day of hot water at 49°C meeting the protocol for hot water use based on the Building America Research Benchmark Definition which aims to capture the living habits and energy use of the average American household. The COP of the WW-GSHP varied from a low value of 2.69 in January when the entering water temperature from the ground loop was 7.42^{o}C, to the highest measured value of 3.57 in July when the entering water temperature was 28.03^{o}C. Reasonably high COPs can be obtained for providing domestic hot water for the average home in the U.S with one single vertical bore that was also shared by a separate GSHP for space conditioning. The best performance relative to a 2-T Carnot system is characterized by $\eta = 0.315$ attained in February (Table **8**) even from a relatively shallow vertical ground loop using 20% (v/v) polypropylene-water mixtures. The maximum efficiency of the WW-GSHP was

32% of the Carnot efficiency (Table **7**). Depending on the season, between 32%-35% of the total electrical energy input to the compressor is rejected as heat to the surroundings as determined from Table **3**. The compressor heat rejected to the conditioned space is marginally beneficial during the heating season but marginally detrimental during the cooling season. However, the net effect is essentially nullified on a year-round basis at least for the geographical region and loads considered in this study. Moreover, the magnitude of the heat rejection (Table **3**) is not large compared to the whole house space conditioning loads. The main sources of systemic inefficiency are the compressor, expansion valve, DHW, and ground loop heat exchangers, with negligible irreversibility in the accompanying connecting lines.

Although the irreversibility rate, $\dot{I}$ (W) is lowest in the winter and highest during the summer (Table **6**), the total irreversibility or lost work, $\dot{I} \times t_{Comp}$ (kWh) is higher in winter than in summer (Table **7**) because of longer compressor run times in the former versus the latter season.

Approximately 68-76% of the total energy input for the WW-GSHP came from the ground, estimated by the ratio, $\dot{Q}_{o,\,ground} \,/\, E_{in}$ (Table **4**). The electrical energy input to the compressor is about 21-28% of the *total* energy input, $W_{e,Comp.}/E_{in}$ (Table **4**). The compressor consumes the largest share of the *electrical* energy input – 88-91% (calculated from Table **3**), whereas the electrical energy consumption of the two pumps and the control system account for less than 3.7% of the total energy input and less than 11% of the total *electrical* energy input (Calculated from Table **3**).

Since 68%-76% of the energy needed to produce domestic hot water can be extracted from the ground (Table **4**), this technology enables practical use of ground thermal energy as a renewable energy resource for domestic water heating.

10. Acknowledgements

The authors would like to thank Brian Fricke, Bo Shen, Bill Miller, W. Blake Hawley and Matthew Mitrani for reviewing this paper and suggesting changes. The research was conducted under a CRADA agreement with ClimateMaster, sponsored by the U.S. Department of Energy's Buildings Technology program.

11. References

[1]. DOE (March 2012). 2011 Buildings Energy Data Book. Energy Efficiency & Renewable Energy Buildings Energy Data Book, Buildings Technologies Program, US Department of Energy: Table 1.1.5.

[2]. DOE (March 2012). 2011 Buildings Energy Data Book. Energy Efficiency & Renewable Energy Buildings Energy Data Book, Buildings Technologies Program, US Department of Energy: Table 1.4.2.

[3]. DOE (March 2012). 2011 Buildings Energy Data Book. Energy Efficiency & Renewable Energy Buildings Energy Data Book, Buildings Technologies Program, US Department of Energy: Table 2.1.6.

[4]. Dumas, P, and Simone, L (Eds.)(2012). Strategic Research Priorities for Geothermal Technology: European Technology Platform on Renewable Heating and Cooling, p.7. http://www.rhc-platform.org/publications/

[5]. McGrath, M. (2014). EU Outlines 2030 climate goals. BBC News, Science and Environment; January 22, 2014; http://www.bbc.com/news/science-environment-25841134

[6]. Sivasakthivel, T., Murugaesan, K., Sahoo, P. K. (2014). A study on energy and CO_2 saving potential of ground source heat pump system in India. Renewable and Sustainable Energy Reviews 32 (2014) 278-293. doi:10.1016/j.rser.2014.01.031

[7]. Bagdanavicius, A., and Jenkins, N, (2013). Power requirements of ground source heat pumps in a residential area; Appl. Energy, 102, 591-600. doi:10.1016/j.apenergy.2012.08.036

[8]. Ozyurt, O., and Ekinci, D. A., (2011). Experimental study of vertical ground-source heat pump performance evaluation for cold climate in Turkey, Appl. Energy 2011;88:1257-65. doi:10.1016/j.apenergy.2010.10.046

[9]. Stuart, J. S., Reddy, B. V., and Rosen, M. A., (2013). Geothermal heat pump systems: Status review and comparison with other heating options, Appl. Energy 101, 341-348. doi:10.1016/j.apenergy.2012.01.048

[10]. Man, Y., Yang, H., Wang, J., and Fang, Z, (2012). In situ operation performance test of ground coupled heat pump system for cooling and heating provision in temperate zone. Appl. Energy 2012; 97:913-20. doi:10.1016/j.apenergy.2011.11.049

[11]. Ozturk, M, (2014). Energy and exergy analysis of a combined ground source heat pump. Appl. Therm. Eng., 73, 362-370. doi:10.1016/j.applthermaleng.2014.08.016

[12]. Xu, G., Zhang, X., Deng, S. (2011). Experimental study on the operating characteristics of a novel low-concentrating solar photovoltaic/thermal integrated heat pump water heating system. Appl. Therm. Eng. 31, (17-18), 3689-3695

[13]. Chen, H., Riffat, S. B., Fu, Y. (2011). Experimental study on a hybrid photovoltaic/heat pump system. Appl. Therm. Eng., 31, 4132-4138.

[14]. Self, S. J., Reddy, B. V., Rosen, M. A. (2013). Ground source heat pumps for heating: parametric energy analysis of a vapor compression cycle utilizing an economizer arrangement, Appl. Therm. Eng. 52, 245-254

[15]. Hazi, A., Hazi, G., Grigore, R., Vernica, S. (2014). Opportunity to use PVT systems for water heating in industry. Appl. Therm. Eng. 63, 151-157.

[16]. Cecchinato L, Corradi M,Fornesieri E, Zamboni L. Carbon dioxide as refrigerant for tap water heat pumps: A comparison with the traditional solution. Int. J. Refrigeration 2005; 28(8): 1250-1258. doi:10.1016/j.ijrefrig.2005.05.019

[17]. Minetto, S. Theoretical and experimental analysis of a CO_2 heat pump for domestic hot water. Int J. of Refrigeration 2011; 34(3): 742-751. doi:10.1016/j.ijrefrig.2010.12.018

[18]. Nanxi L, L. Shi L, Lizhong H, Mingshan Z. Moderately high temperature water source heat-pumps using a near-azeotropic refrigerant mixture. Applied Energy 2005; 80(4): 435-447. doi:10.1016/j.apenergy.2004.02.005

[19]. Neksa P, Rekstad H, Zakeri GR, Schiefloe PA. CO_2-heat pump water heater: characteristics, system design and experimental results. Int J. Refrig. 1998;21(No. 3): 172-179. doi:10.1016/S0140-7007(98)00017-6

[20]. Stene J. Residential CO_2 heat pump system for combined space heating and hot water heating. Int. J. Refrigeration. 2005;28(8): 1259-1265. doi:10.1016/j.ijrefrig.2005.07.006

[21]. Yang, H., Cui, P., and Fang, Z; (2012). Vertical-borehole ground-coupled heat pumps: A review of models and systems; Applied Energy, Vol. 87, Issue 1:16-27. doi:10.1016/j.apenergy.2009.04.038

[22]. Ally MR, Munk JD, Baxter VD, Gehl AC. Exergy and energy analysis of a ground-source heat pump for domestic water heating under simulated occupancy conditions. Int. J. Refrig. 2013:36,5,1417-1430. http://dx.doi.org/10.1016/j.ijrefrig.2013.03.006

[23]. Ally MR, Munk JD, Baxter VD, Gehl AC. Exergy analysis and operational efficiency of a horizontal ground-source heat pump system operated in a low-energy test house under simulated occupancy conditions. Int. J. Refrig. 2012:35,4,1092-1103. http://dx.doi.org/10.1016/j.ijrefrig.2012.01.013

[24]. Hendron, R. and C. Engebrecht (2010). Building America Research Benchmark Definition., National Renewable Energy Laboratory. NREL/TP-550-47246. http://www.nrel.gov/docs/fy10osti/47246.pdf.

[25]. Lemmon, E.W., Huber, M.L., McLinden, M.O. NIST Standard Reference Database 23: Reference Fluid Thermodynamic and Transport Properties-REFPROP, Version 8.0, National Institute of Standards and Technology, Standard Reference Data Program, Gaithersburg, April 2007.

[26]. Warke Jr., K. (1995). Advanced Thermodynamics for Engineers, McGraw-Hill, New York, ISBN 0-07-068292-5.

[27]. Myers, G. E. (2007). Engineering Thermodynamics, 2nd ed.,AMCHT Publications, ISBN 978-0-9666065-2-2.

[28]. Ally, M., Munk, J., Baxter, V., Gehl, A., (2014). Measured water heating performance of a vertical-bore water-to-water ground source heat pump (WW-GSHP) for domestic water heating over twelve months under simulated occupancy loads. 11th IEA Heat Pump Conference, Montreal, Canada, May 12-14, 2014, P1.2

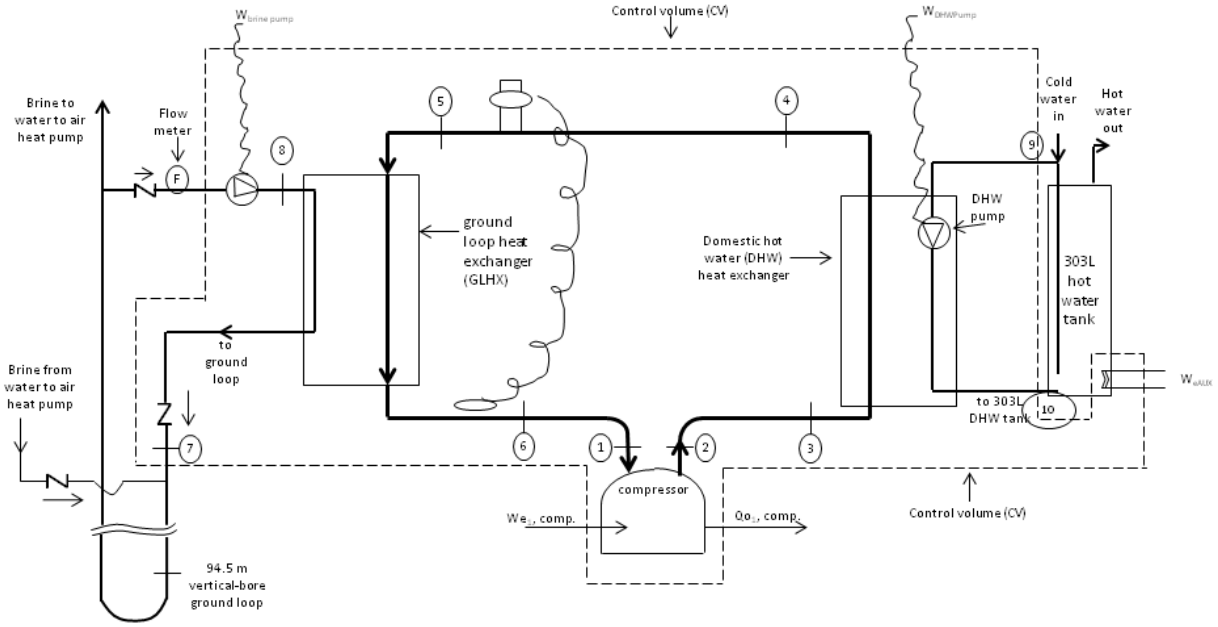

Figure 1. Schematic of the shared vertical-bore and WW-GSHP components for producing domestic hot water. Numbered items show state points where measurements were taken.

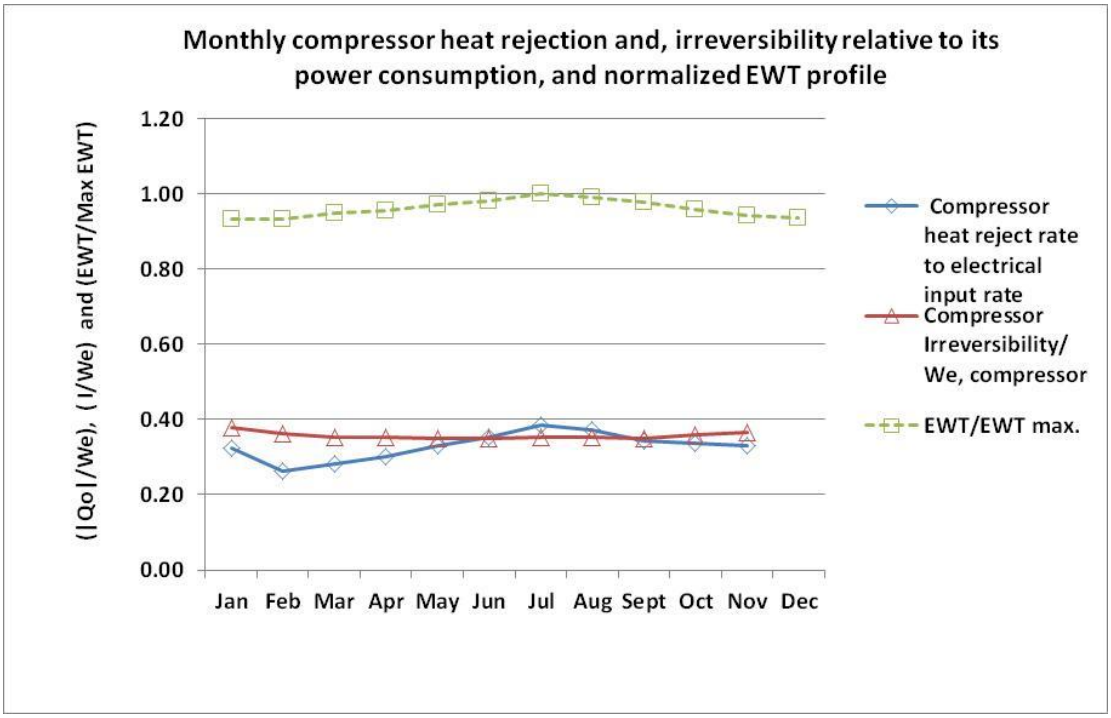

Figure 2. Compressor heat rejection and irreversibility per unit electrical input and normalized EWT for each month in 2012.

Figure Captions

Figure 1. Schematic of the shared vertical-bore and WW-GSHP components for producing domestic hot water. Numbered items show state points where measurements were taken.

Figure 2. Compressor heat rejection and irreversibility per unit electrical input and normalized EWT for each month in 2012.

Table 1. Water use schedule and duration under simulated occupancy conditions[1].

Shower Schedule		Clothes Washer Schedule			Dishwasher Schedule		
Start Times (24 h basis)	**Daily Water Use Liters (L)**	**Start Times (24 h basis)**	**Days**	**Daily Water Use Liters(L)**	**Start Times (24 h basis)**	**Days**	**Liters(L)**
7:00:00 AM	75.71	7:30:00 AM	Thurs	13.93	7:30:00 PM	Mon	15.29
8:30:00 AM	18.93	5:15:00 PM	Thurs	13.93	7:30:00 PM	Tues	15.29
12:00:00 PM	18.93	8:00:00 AM	Tues/ Wed	13.9/13.9	7:30:00 PM	Wed	15.29
5:00:00 PM	37.85	10:00:00 AM	Tues/ Wed	13.9/13.9	7:30:00 PM	Thurs	15.29
9:00:00 PM	75.71						

[1] Shower used mixed hot and cold water at approximately 40.6^{o}C (105^{o}F); clothes washer and dishwasher used hot water at approximately 49^{o}C (120^{o}F)

Table 2. Energy transfer and irreversibility rates calculated from averaged monthly measured thermodynamic properties at the given state points for the WW-GSHP.Energy transfer and irreversibility rates calculated from averaged monthly measured thermodynamic properties at the given state points for the WW-GSHP.

	Compressor																		
	Discharge (Final state:(2))				Suction (Initial state: (1))														
	T	P	h	s	T	P	h	s	$\dot{Q}_o$	$\dot{W}_e$	$\dot{m}_{map}$	$\dot{m}_{r,DHW}$	$\%\Delta_1$	$\dot{m}_{r,b}$	$\%\Delta_2$	$\dot{\sigma}$	$\dot{I}$	T_o	Run Time
	(°C)	(kPa)	(kJ/kg)	kJ/kg K	(°C)	(kPa)	(kJ/kg)	kJ/kg K	(W)	(W)	(kg/s)	(kg/s)		(kg/s)		(W/K)	(W)	(K)	(hrs)
Jan	81.4	2912.4	331.04	1.08218	6.2	706.3	287.00	1.06957	-434.1	1346.0	0.020707	0.020748	0.20%	0.01990	-3.88%	1.735	512	294.87	90.292
Feb	81.5	2913.8	331.27	1.08219	7.0	718.8	286.49	1.06170	-352.4	1349.1	0.022259	0.021254	-4.52%	0.02041	-8.32%	1.653	487	294.84	83.113
Mar	80.7	3006.8	328.89	1.07297	11.6	813.5	288.93	1.05992	-389.7	1379.7	0.024776	0.023148	-6.57%	0.02041	-17.63%	1.641	486	296.17	73.200
Apr	80.2	3051.5	469.78	1.84161	13.2	850.1	432.04	1.83286	-421.6	1392.4	0.025724	0.023759	-7.64%	0.02322	-9.74%	1.647	489	296.93	62.133
May	80.1	3092.4	469.11	1.83873	17.9	930.1	435.07	1.83561	-462.7	1404.8	0.027684	0.025610	-7.49%	0.02435	-12.05%	1.647	489	296.87	58.058
Jun	80.9	3117.0	469.57	1.83915	21.2	974.3	437.58	1.83996	-499.6	1415.7	0.028640	0.026367	-7.93%	0.02512	-12.28%	1.659	493	297.43	49.400
Jul	82.5	3139.4	471.33	1.84379	26.2	1034.9	441.73	1.84892	-546.5	1425.1	0.029675	0.028281	-4.70%	0.02675	-9.85%	1.684	502	297.98	46.400
Aug	81.7	3123.0	470.55	1.84218	23.6	1003.8	439.73	1.84547	-526.1	1417.3	0.028917	0.027282	-5.65%	0.02609	-9.78%	1.678	498	297.01	50.500
Sept	80.8	3091.3	469.92	1.84102	20.3	956.8	437.08	1.84000	-483.9	1409.1	0.028179	0.026087	-7.42%	0.02521	-10.53%	1.660	493	297.01	50.375
Oct	79.6	3039.7	469.38	1.84132	14.1	861.7	433.12	1.83740	-467.4	1389.8	0.025435	0.023755	-6.61%	0.02328	-8.49%	1.683	497	295.52	61.458
Nov	79.9	2985.0	470.56	1.84612	9.4	770.8	430.61	1.83933	-451.5	1362.6	0.022804	0.022053	-3.30%	0.02145	-5.93%	1.682	498	296.07	70.667
Dec	80.1	2993.0	471.22	1.84881	7.7	746.1	429.72	1.84060	-444.6	1350.6	0.021832	0.022503	3.07%	0.02158	-1.17%	1.688	498	294.94	78.350

	Refrigerant Line from Compressor Discharge to DHW HX																		
	Final state point: (3)				Initial state point: (2)													Rectified	
	T	P	h	s	T	P	h	s	$\dot{Q}_o$ †	$\dot{W}_e$	$\dot{m}_{map}$	$\dot{m}_{r,DHW}$	$\%\Delta_1$	$\dot{m}_{r,b}$	$\%\Delta_2$	$\dot{\sigma}$	$\dot{I}$	T_o	
	(°C)	(kPa)	(kJ/kg)	kJ/kg K	(°C)	(kPa)	(kJ/kg)	kJ/kg K	(W)	(W)	(kg/s)	(kg/s)		(kg/s)		(W/K)	(W)	(K)	
Jan	80.0	2905.4	329.96	1.07961	81.4	2912.4	331.04	1.08218	-22.2	0.0	0.020707	0.020748	0.20%	0.01990	-3.88%	0.02211	6.52	294.87	
Feb	80.0	2905.8	329.43	1.07708	81.5	2913.8	331.27	1.08219	-41.0	0.0	0.022259	0.021254	-4.52%	0.02041	-8.32%	0.02526	7.45	294.84	
Mar	79.4	2992.9	326.44	1.06579	80.7	3006.8	328.89	1.07297	-60.7	0.0	0.024776	0.023148	-6.57%	0.02041	-17.63%	0.0268	7.94	296.17	
Apr	79.0	3035.2	467.97	1.83655	80.2	3051.5	469.78	1.84161	-46.3	0.0	0.025724	0.023759	-7.64%	0.02322	-9.74%	0.02594	7.70	296.93	
May	78.9	3074.2	467.39	1.83392	80.1	3092.4	469.11	1.83873	-47.5	0.0	0.027684	0.025610	-7.49%	0.02435	-12.05%	0.02668	7.92	296.87	
Jun	79.7	3107.0	467.87	1.83440	80.9	3117.0	469.57	1.83915	-48.6	0.0	0.028640	0.026367	-7.93%	0.02512	-12.28%	0.02743	8.16	297.43	
Jul	81.3	3119.5	468.94	1.83685	82.5	3139.4	471.33	1.84379	-71.0	0.0	0.029675	0.028281	-4.70%	0.02675	-9.85%	0.03242	9.66	297.98	
Aug	80.4	3102.4	468.76	1.83716	81.7	3123.0	470.55	1.84218	-51.8	0.0	0.028917	0.027282	-5.65%	0.02609	-9.78%	0.029	8.61	297.01	
Sept	79.5	3075.1	468.24	1.83635	80.8	3091.3	469.92	1.84102	-47.2	0.0	0.028179	0.026087	-7.42%	0.02521	-10.53%	0.02743	8.15	297.01	
Oct	78.3	3023.0	467.59	1.83629	79.6	3039.7	469.38	1.84132	-45.6	0.0	0.025435	0.023755	-6.61%	0.02328	-8.49%	0.02633	7.78	295.52	
Nov	78.5	2971.4	468.70	1.84094	79.9	2985.0	470.56	1.84612	-42.3	0.0	0.022804	0.022053	-3.30%	0.02145	-5.93%	0.02491	7.38	296.07	
Dec	78.6	2950.9	469.31	1.84346	80.1	2993.0	471.22	1.84881	-41.8	0.0	0.021832	0.022503	3.07%	0.02062	-5.55%	0.02506	7.39	294.94	

† $\dot{Q}_o$ should be zero. Postive values reflect errors in temperature measurement. The rectified entropy production and irreversibility are calculated assuming adiabatic conditons. See text for explanations

Table 2 (continued).

Refrigerant-DHW Heat Exchanger

	Final state point:(4)				Initial state point: (3)													
	T	P	h	s	T	P	h	s	$\dot{Q}_o$	$\dot{W}_e$	$\dot{m}_{map}$	$\dot{m}_{r,DHW}$	$\%\Delta_1$	$\dot{m}_{r,b}$	$\%\Delta_2$	$\dot{\sigma}$	$\dot{I}$	T_o
	(^{o}C)	(kPa)	(kJ/kg)	kJ/kg K	(^{o}C)	(kPa)	(kJ/kg)	kJ/kg K	(W)	(W)	(kg/s)	(kg/s)		(kg/s)		(W/K)	(W)	(K)
Jan	42.5	2885.1	128.65	0.45990	80.0	2905.4	329.96	1.07961	-4168.6	0.0	0.020707	0.020748	0.20%	0.01990	-3.88%	0.285	91	317.80
Feb	42.4	2885.5	128.40	0.45897	80.0	2905.8	329.43	1.07708	-4474.7	0.0	0.022259	0.021254	-4.52%	0.02041	-8.32%	0.326	104	317.70
Mar	43.3	2971.9	130.03	0.46390	79.4	2992.9	326.44	1.06579	-4866.2	0.0	0.024776	0.023148	-6.57%	0.02041	-17.63%	0.359	114	318.64
Apr	43.8	3013.9	273.19	1.24045	79.0	3035.2	467.97	1.83655	-5010.7	0.0	0.025724	0.023759	-7.64%	0.02322	-9.74%	0.365	117	319.16
May	44.0	3052.7	273.55	1.24149	78.9	3074.2	467.39	1.83392	-5366.4	0.0	0.027684	0.025610	-7.49%	0.02435	-12.05%	0.399	127	319.42
Jun	44.4	3085.3	274.17	1.24337	79.7	3107.0	467.87	1.83440	-5547.4	0.0	0.028640	0.026367	-7.93%	0.02512	-12.28%	0.423	135	319.73
Jul	44.3	3097.7	274.06	1.24295	81.3	3119.5	468.94	1.83685	-5783.2	0.0	0.029675	0.028281	-4.70%	0.02675	-9.85%	0.465	149	319.70
Aug	44.1	3080.7	273.70	1.24190	80.4	3102.4	468.76	1.83716	-5640.3	0.0	0.028917	0.027282	-5.65%	0.02609	-9.78%	0.439	140	319.53
Sept	43.9	3053.6	273.30	1.24072	79.5	3075.1	468.24	1.83635	-5493.0	0.0	0.028179	0.026087	-7.42%	0.02521	-10.53%	0.421	134	319.27
Oct	43.5	3001.8	272.67	1.23892	78.3	3023.0	467.59	1.83629	-4957.9	0.0	0.025435	0.023755	-6.61%	0.02328	-8.49%	0.352	112	318.91
Nov	43.2	2950.6	272.13	1.23740	78.5	2971.4	468.70	1.84094	-4482.7	0.0	0.022804	0.022053	-3.30%	0.02145	-5.93%	0.310	99	318.51
Dec	43.1	2930.2	271.89	1.23672	78.6	2950.9	469.31	1.84346	-4309.9	0.0	0.021832	0.022503	3.07%	0.02158	-1.17%	0.291	93	318.36

Expansion Valve and connecting lines

	Final state: (5)				Initial state:(4)													
	T	P	h	s	T	P	h	s	$\dot{Q}_o$	$\dot{W}_e$	$\dot{m}_{map}$	$\dot{m}_{r,DHW}$	$\%\Delta_1$	$\dot{m}_{r,b}$	$\%\Delta_2$	$\dot{\sigma}$	$\dot{I}$	T_o
	(^{o}C)	(kPa)	(kJ/kg)	kJ/kg K	(^{o}C)	(kPa)	(kJ/kg)	kJ/kg K	(W)	(W)	(kg/s)	(kg/s)		(kg/s)		(W/K)	(W)	(K)
Jan	-1.1	710.9	128.65	0.48719	42.5	2885.1	128.65	0.45990	0.0	0.0	0.020707	0.020748	0.20%	0.01990	-3.88%	0.565	167	294.87
Feb	0.8	723.4	128.40	0.48429	42.4	2885.5	128.40	0.45897	0.0	0.0	0.022259	0.021254	-4.52%	0.02041	-8.32%	0.563	166	294.84
Mar	4.2	817.3	130.03	0.48689	43.3	2971.9	130.03	0.46390	0.0	0.0	0.024776	0.023148	-6.57%	0.02041	-17.63%	0.569	169	296.17
Apr	5.5	852.9	273.19	1.26269	43.8	3013.9	273.19	1.24045	0.0	0.0	0.025724	0.023759	-7.64%	0.02322	-9.74%	0.572	170	296.93
May	8.2	933.4	273.55	1.26156	44.0	3052.7	273.55	1.24149	0.0	0.0	0.027684	0.025610	-7.49%	0.02435	-12.05%	0.555	165	296.87
Jun	9.7	979.6	274.17	1.26249	44.4	3085.3	274.17	1.24337	0.0	0.0	0.028640	0.026367	-7.93%	0.02512	-12.28%	0.547	163	297.43
July	11.4	1037.5	274.06	1.26058	44.3	3097.7	274.06	1.24295	0.0	0.0	0.029675	0.028281	-4.70%	0.02675	-9.85%	0.523	156	297.98
Aug	10.3	1006.2	273.70	1.26026	44.1	3080.7	273.70	1.24190	0.0	0.0	0.028917	0.027282	-5.65%	0.02609	-9.78%	0.531	158	297.01
Sept	9.1	960.4	273.30	1.25993	43.9	3053.6	273.30	1.24072	0.0	0.0	0.028179	0.026087	-7.42%	0.02521	-10.53%	0.541	161	297.01
Oct	5.3	865.1	272.67	1.26107	43.5	3001.8	272.67	1.23892	0.0	0.0	0.025435	0.023755	-6.61%	0.02328	-8.49%	0.563	166	295.52
Nov	1.7	774.1	272.13	1.26256	43.2	2950.6	272.13	1.23740	0.0	0.0	0.022804	0.022053	-3.30%	0.02145	-5.93%	0.574	170	296.07
Dec	0.3	744.1	271.89	1.26316	43.1	2930.2	271.89	1.23672	0.0	0.0	0.021832	0.022503	3.07%	0.02158	-1.17%	0.577	170	294.94

Table 2 (continued).

Refrigerant-Brine GL HX

	Final state point:(6)				Initial state point:(5)													
	T	P	h	s	T	P	h	s	$\dot{Q}_o$	$\dot{W}_e$	$\dot{m}_{map}$	$\dot{m}_{r,DHW}$	$\%\Delta_1$	$\dot{m}_{r,b}$	$\%\Delta_2$	$\dot{\sigma}$	$\dot{I}$	T_o
	(°C)	(kPa)	(kJ/kg)	kJ/kg K	(°C)	(kPa)	(kJ/kg)	kJ/kg K	(W)	(W)	(kg/s)	(kg/s)		(kg/s)		(W/K)	(W)	(K)
Jan	7.8	705.9	288.59	1.07517	-1.1	710.9	128.65	0.48719	3311.9	0.0	0.020707	0.020748	0.20%	0.01984	-4.17%	0.304	85	278.99
Feb	8.5	718.3	288.13	1.06745	0.8	723.4	128.40	0.48429	3555.5	0.0	0.022259	0.021254	-4.52%	0.01997	-10.29%	0.270	76	279.73
Mar	13.1	811.5	290.51	1.06538	4.2	817.3	130.03	0.48689	3976.1	0.0	0.024776	0.023148	-6.57%	0.02010	-18.89%	0.342	97	284.21
Apr	14.8	846.9	433.69	1.83855	5.5	852.9	273.19	1.26269	4128.8	0.0	0.025724	0.023759	-7.64%	0.02022	-21.39%	0.375	107	285.97
May	19.3	926.9	436.58	1.84068	8.2	933.4	273.55	1.26156	4513.3	0.0	0.027684	0.025610	-7.49%	0.02035	-26.50%	0.490	142	290.40
Jun	22.6	972.7	439.06	1.84488	9.7	979.6	274.17	1.26249	4722.2	0.0	0.028640	0.026367	-7.93%	0.02047	-28.51%	0.580	170	293.32
Jul	27.5	1030.2	443.09	1.85338	11.4	1037.5	274.06	1.26058	5016.2	0.0	0.029675	0.028281	-4.70%	0.02060	-30.58%	0.701	208	296.98
Aug	25.0	999.1	441.16	1.85019	10.3	1006.2	273.70	1.26026	4842.3	0.0	0.028917	0.027282	-5.65%	0.02073	-28.33%	0.660	195	295.29
Sept	21.8	953.7	438.62	1.84515	9.1	960.4	273.30	1.25993	4658.5	0.0	0.028179	0.026087	-7.42%	0.02085	-26.00%	0.571	167	292.64
Oct	15.7	859.0	434.79	1.84313	5.3	865.1	272.67	1.26107	4123.7	0.0	0.025435	0.023755	-6.61%	0.02098	-17.53%	0.432	124	286.91
Nov	11.0	768.7	432.26	1.84507	1.7	774.1	272.13	1.26256	3651.6	0.0	0.022804	0.022053	-3.30%	0.02110	-7.46%	0.343	97	282.18
Dec	9.4	738.9	431.50	1.84683	0.3	744.1	271.89	1.26316	3484.6	0.0	0.021832	0.022503	3.07%	0.02123	-2.76%	0.324	91	280.58

Refrigerant Line from Refrigerant-Brine GL HX to Compressor Suction

	Final state point:(1)				Initial state point:(6)													
	T	P	h	s	T	P	h	s	$\dot{Q}_o$	$\dot{W}_e$	$\dot{m}_{map}$	$\dot{m}_{r,DHW}$	$\%\Delta_1$	$\dot{m}_{r,b}$	$\%\Delta_2$	$\dot{\sigma}$	$\dot{I}$	T_o
	(°C)	(kPa)	(kJ/kg)	kJ/kg K	(°C)	(kPa)	(kJ/kg)	kJ/kg K	(W)	(W)	(kg/s)	(kg/s)		(kg/s)		(W/K)	(W)	(K)
Jan	6.2	706.3	287.00	1.06957	7.8	705.9	288.59	1.07517	-33.0	0.0	0.020707	0.020748	0.20%	0.01990	-3.88%	-0.004	-1.21	294.87
Feb	7.0	718.8	286.49	1.06170	8.5	718.3	288.13	1.06745	-36.5	0.0	0.022259	0.021254	-4.52%	0.02041	-8.32%	-0.004	-1.26	294.84
Mar	11.6	813.5	288.93	1.05992	13.1	811.5	290.51	1.06538	-39.2	0.0	0.024776	0.023148	-6.57%	0.02041	-17.63%	-0.003	-0.88	296.17
Apr	13.2	850.1	432.04	1.83286	14.8	846.9	433.69	1.83855	-42.7	0.0	0.025724	0.023759	-7.64%	0.02322	-9.74%	-0.003	-0.83	296.93
May	17.9	930.1	435.07	1.83561	19.3	926.9	436.58	1.84068	-41.6	0.0	0.027684	0.025610	-7.49%	0.02435	-12.05%	0.000	-0.07	296.87
Jun	21.2	974.3	437.58	1.83996	22.6	972.7	439.06	1.84488	-42.2	0.0	0.028640	0.026367	-7.93%	0.02512	-12.28%	0.001	0.35	297.43
Jul	26.2	1034.9	441.73	1.84892	27.5	1030.2	443.09	1.85338	-40.5	0.0	0.029675	0.028281	-4.70%	0.02675	-9.85%	0.003	1.02	297.98
Aug	23.6	1003.8	439.73	1.84547	25.0	999.1	441.16	1.85019	-41.3	0.0	0.028917	0.027282	-5.65%	0.02609	-9.78%	0.003	0.78	297.01
Sept	20.3	956.8	437.08	1.84000	21.8	953.7	438.62	1.84515	-43.4	0.0	0.028179	0.026087	-7.42%	0.02521	-10.53%	0.001	0.26	297.01
Oct	14.1	861.7	433.12	1.83740	15.7	859.0	434.79	1.84313	-42.6	0.0	0.025435	0.023755	-6.61%	0.02328	-8.49%	-0.002	-0.47	295.52
Nov	9.4	770.8	430.61	1.83933	11.0	768.7	432.26	1.84507	-37.6	0.0	0.022804	0.022053	-3.30%	0.02145	-5.93%	-0.004	-1.10	296.07
Dec	7.7	746.1	429.72	1.84060	9.4	738.9	431.50	1.84683	-38.8	0.0	0.021832	0.022503	3.07%	0.02158	-1.17%	-0.004	-1.30	294.94

Table 3. Monthly energy balances and coefficient of performance of the WW-GSHP.

2012	$W_{e,\ Brine\ Pump}$ (kWh)	$W_{e,\ Compressor}$ (kWh)	$W_{e,\ DHW\ Pump}$ (kWh)	$W_{e,\ Aux}$ (kWh)	$W_{e,\ Controls}$ (kWh)	Total Electrical Energy In (kWh)	$Q_{o,\ ground}$ (kWh)	Q_{DHW} (kWh)	$Q_{o,\ Comp.}$ (kWh)	Total Energy In (E_{in}) (kWh)	Total Energy Out (E_{out}) (kWh)	$\%\Delta=100[(E_{in}-\lvert E_{out}\rvert)/E_{in}]$
Jan	12.01	121.54	4.51	0.00	1.984	140.03	298.84	-376.14	-39.25	438.87	-415.39	5.35%
Feb	11.13	112.13	4.16	0.00	1.832	129.25	295.31	-371.66	-29.35	424.56	-401.00	5.55%
Mar	9.81	100.99	3.63	0.00	1.665	116.09	290.86	-355.97	-28.57	406.95	-384.54	5.51%
Apr	8.31	86.51	3.07	0.00	1.523	99.42	256.37	-311.12	-26.24	355.78	-337.36	5.18%
May	7.57	81.56	2.84	0.00	1.377	93.35	261.86	-311.35	-26.90	355.21	-338.25	4.77%
Jun	6.25	69.94	2.41	0.00	1.224	79.83	233.12	-273.86	-24.71	312.95	-298.57	4.59%
Jul	5.49	66.12	2.28	0.00	1.191	75.09	232.60	-268.16	-25.39	307.68	-293.55	4.59%
Aug	6.20	71.57	2.48	0.00	1.273	81.53	244.37	-284.65	-26.60	325.90	-311.24	4.50%
Sept	6.46	70.98	2.47	0.00	1.216	81.14	234.51	-276.53	-24.41	315.65	-300.94	4.66%
Oct	8.20	85.42	3.03	0.00	1.479	98.13	253.27	-304.50	-28.77	351.39	-333.27	5.16%
Nov	9.33	96.29	3.48	0.00	1.596	110.70	257.87	-316.56	-31.95	368.57	-348.51	5.44%
Dec	10.34	105.82	3.86	0.08	1.734	121.75	272.83	-337.46	-34.88	394.67	-372.34	5.66%

Table 4. Water heating COP, brine temperatures, compressor run times, and the fraction of total water heating energy required that is extracted from the ground

2012	LWT (^{o}C)	EWT (^{o}C)	COP	$\frac{W_{e,Comp}}{E_{in}}$ (%)	$\frac{Q_{o,ground}}{E_{in}}$ (%)	Compressor Run time (hrs)	$\lvert Q_{DHW} \rvert$ (kWh)	$\%Q_{GLHX} / \lvert Q_{DHW} \rvert$
Jan	4.24	7.43	2.69	28%	68%	90.29	376.1	79.4%
Feb	5.05	8.12	2.88	26%	70%	83.11	371.7	79.5%
Mar	9.50	12.61	3.07	25%	71%	73.20	356.0	81.7%
Apr	11.27	14.36	3.13	24%	72%	62.13	311.1	82.4%
May	15.40	19.09	3.34	23%	74%	58.06	311.4	84.1%
Jun	17.75	22.58	3.43	22%	74%	49.40	273.9	85.1%
Jul	19.64	28.03	3.57	21%	76%	46.40	268.2	86.7%
Aug	19.14	25.14	3.49	22%	75%	50.50	284.6	85.9%
Sept	17.27	21.70	3.41	22%	74%	50.38	276.5	84.8%
Oct	12.20	15.33	3.10	24%	72%	61.46	304.5	83.2%
Nov	7.40	10.66	2.86	26%	70%	70.67	316.6	81.5%
Dec	5.83	9.03	2.77	27%	69%	78.35	337.5	80.8%

Table 5. Monthly compressor run times and temperatures required to calculate the monthly irreversibility and the energy and entropy balances around The GL HX and the DHW HX.

	T_9 (K)	T_{10} (K)	LWT (K)	EWT (K)	Comp. Run Time (hrs)
Jan	315.4	320.2	277.4	280.6	90.292
Feb	315.2	320.2	278.2	281.3	83.113
Mar	316.0	321.3	282.7	285.8	73.200
Apr	316.4	321.9	284.4	287.5	62.133
May	316.5	322.4	288.5	292.2	58.058
Jun	316.7	322.8	290.9	295.7	49.400
Jul	316.5	322.9	292.8	301.2	46.400
Aug	316.4	322.7	292.3	298.3	50.500
Sept	316.3	322.3	290.4	294.8	50.375
Oct	316.1	321.7	285.4	288.5	61.458
Nov	316.0	321.1	280.5	283.8	70.667
Dec	315.9	320.9	279.0	282.2	78.350

Table 6 Entropy production and irreversibility rates between state points in the closed refrigeration cycle and contributing components.

	Compressor	Compressor Discharge to DHW HX	DHW HX	Expansion Valve & connecting lines	Refrig.-Brine GL HX	Ref.-Brine GL HX to Compressor sucton	Total
State points →	[1→2]	[2→3]	[3→4]	[4→5]	[5→6]	[6→1]	
	$\dot{\sigma}$ (W·K^{-1})	$\dot{\sigma}$ (W·K^{-1})	$\dot{\sigma}$ (W·K^{-1})	$\dot{\sigma}$ (W·K^{-1})	$\dot{\sigma}$ (W·K^{-1})	$\dot{\sigma}$ (W·K^{-1})	$\dot{\sigma}$ (W·K^{-1})
Jan	1.7352	0.0221	0.2848	0.5647	0.3038	-0.0041	2.9065
Feb	1.6534	0.0253	0.3258	0.5631	0.2703	-0.0043	2.8336
Mar	1.6412	0.0268	0.3590	0.5692	0.3425	-0.0030	2.9357
Apr	1.6470	0.0259	0.3651	0.5718	0.3749	-0.0028	2.9819
May	1.6470	0.0267	0.3990	0.5555	0.4904	-0.0002	3.1183
Jun	1.6588	0.0274	0.4231	0.5474	0.5796	0.0012	3.2375
Jul	1.6839	0.0324	0.4653	0.5226	0.7009	0.0034	3.4086
Aug	1.6783	0.0290	0.4391	0.5307	0.6597	0.0026	3.3394
Sept	1.6602	0.0274	0.4207	0.5409	0.5714	0.0009	3.2215
Oct	1.6834	0.0263	0.3524	0.5630	0.4317	-0.0016	3.0553
Nov	1.6817	0.0249	0.3101	0.5735	0.3429	-0.0037	2.9293
Dec	1.6885	0.0251	0.2912	0.5769	0.3236	-0.0044	2.9007

	Compressor	Compressor Discharge to DHW HX	DHW HX	Expansion Valve & connecting lines	Refrig.-Brine GL HX	Ref.-Brine GL HX to Compressor sucton	Total
State points →	[1→2]	[2→3]	[3→4]	[4→5]	[5→6]	[6→1]	
	$\dot{I}$ (W)	$\dot{I}$ (W)	$\dot{I}$ (W)	$\dot{I}$ (W)	$\dot{I}$ (W)	$\dot{I}$ (W)	$\dot{I}$ (W)
Jan	512	6.52	91	167	85	-1.21	859
Feb	487	7.45	104	166	76	-1.26	839
Mar	486	7.94	114	169	97	-0.88	873
Apr	489	7.70	117	170	107	-0.83	889
May	489	7.92	127	165	142	-0.07	932
Jun	493	8.16	135	163	170	0.35	970
Jul	502	9.66	149	156	208	1.02	1025
Aug	498	8.61	140	158	195	0.78	1001
Sept	493	8.15	134	161	167	0.26	964
Oct	497	7.78	112	166	124	-0.47	907
Nov	498	7.38	99	170	97	-1.10	869
Dec	498	7.39	93	170	91	-1.30	858

Table 7. Monthly total irreversibility, or lost work, given by $\dot{I} \times t_{Comp.}$

	Comp. Run time, $t_{Comp.}$ (hrs)	$\dot{I}$ (W)	$\dot{I}$ x ($t_{Comp.}$) (kWh)
Jan	90.29	858.7	77.5
Feb	83.11	838.8	69.7
Mar	73.20	873.4	63.9
Apr	62.13	889.4	55.3
May	58.06	931.5	54.1
Jun	49.40	969.9	47.9
Jul	46.40	1025.1	47.6
Aug	50.50	1000.6	50.5
Sept	50.38	963.7	48.5
Oct	61.46	907.4	55.8
Nov	70.67	869.4	61.4
Dec	78.35	857.7	67.2

Table 8. Validity and goodness of irreversibility (lost work) calculations

	$\dot{\sigma}_{Total}$ (W·K^{-1})	$\dot{I}_{Total}$ (W)	$\dot{Q}_{Brine\ \ GL\ \ HX}$ (W)	COP_{Carnot}	$\dot{W}_{Carnot}$ (W)	$\dot{W}_{Carnot} + \dot{I}_{Total}$ (W)	$\dot{W}_{Comp.meas.}$ (W)	$\eta = \dot{W}_{Carnot} / \dot{W}_{Comp.meas.}$	%Δ
Jan	2.906	859	3311.9	8.188	404.5	1263.2	1346.0	0.300	-6.56
Feb	2.834	839	3555.5	8.367	424.9	1263.7	1349.1	0.315	-6.76
Mar	2.936	873	3976.1	9.253	429.7	1303.1	1379.7	0.311	-5.88
Apr	2.982	889	4128.8	9.615	429.4	1318.8	1392.4	0.308	-5.58
May	3.118	932	4513.3	11.006	410.1	1341.6	1404.8	0.292	-4.71
Jun	3.237	970	4722.2	12.106	390.1	1360.0	1415.7	0.276	-4.10
Jul	3.409	1025	5016.2	14.076	356.4	1381.4	1425.1	0.250	-3.16
Aug	3.339	1001	4842.3	13.183	367.3	1367.9	1417.3	0.259	-3.61
Sept	3.221	964	4658.5	11.988	388.6	1352.3	1409.1	0.276	-4.20
Oct	3.055	907	4123.7	9.969	413.7	1321.1	1389.8	0.298	-5.20
Nov	2.929	869	3651.6	8.766	416.6	1286.0	1362.6	0.306	-5.95
Dec	2.901	858	3484.6	8.427	413.5	1271.2	1350.6	0.306	-6.25